Original Article

Institution of MECHANICAL ENGINEERS

Journal of AUTOMOBILE ENGINEERING

Proc IMechE Part D:
J Automobile Engineering
1–17

DOI: 10.1177/0954407019845253
journals.sagepub.com/home/pid
SAGE

Trajectory planning and combined control design for critical high-speed lane change manoeuvres

Hadi Sazgar, Shahram Azadi and Reza Kazemi

Abstract

The purpose of this research is to develop an advanced driver assistance system for the integrated longitudinal and lateral guidance of vehicles in critical high-speed lane change manoeuvres. The system consists of two parts: trajectory planning and combined control. At the first, by considering the TV position and the available range of longitudinal acceleration, several trajectories with different accelerations are generated. Then, by taking into account the vehicle and tyre dynamics, the most appropriate trajectory is selected. Therefore, the chosen trajectory is collision free and dynamically feasible. Because the trajectory planning is carried out algebraically, it has low computational cost. This is especially valuable in the experimental implementations. At the second part of the study, using a robust combined longitudinal-lateral controller, the control inputs are determined and transmitted to the brake/throttle and steering actuators. Both in the trajectory planning and combined control design, the nonlinear tyre dynamics and the dynamics of throttle and brake actuators are considered. To evaluate the performance of the proposed guidance algorithm, a full CarSim dynamic model is utilized. The simulation results for critical high-speed lane change manoeuvres confirm that the proposed trajectory planning method works effectively. The tracking error is also very small and the yaw stability is guaranteed.

Keywords

Advanced driver assistant system, high-speed driving, trajectory planning, combined longitudinal and lateral control, nonlinear tyre dynamic

Date received: 30 August 2018; accepted: 25 March 2019

Introduction

Today, the application and capabilities of advanced driver assistance systems (ADAS) are dramatically increasing. ADAS make passengers comfortable, and help in traffic reduction, lower fuel consumption and decrease in pollution. Moreover, they have an important role in reducing car accidents. Worldwide, more than 1.25 million people die as a result of road traffic crashes, and between 20 million and 50 million people are injured every year.[1] The World Health Organization's (WHO) reports also state that about 80% of accidents are caused by human error.[2] One of the common solutions to decrease human error is automatic driving. Although the ultimate goal of an automobile manufacturer is fully automated cars, unmanned driving is a complex problem that has many challenging aspects. In the past decades, numerous and various driver assistance systems have been developed to reduce the impact of driver error and manage hazardous driving situations.[3,4] Majority of available ADAS are related to either the longitudinal or lateral guidance. In other words, there are a few driver assistance systems that can cover both longitudinal and lateral guidance. These few ADAS still have limitations and are useful for normal manoeuvres. Integrated automated guidance has many subjects of research. The main focus of this article is on trajectory planning and integrated control design. In the following, a summarized literature review will be presented.

Department of Mechanical Engineering, K. N. Toosi University of Technology, Tehran, Iran

Corresponding author:
Hadi Sazgar, Department of Mechanical Engineering, K. N. Toosi University of Technology, No. 7, Pardis St., Mollasadra Ave., Vanak Square, Tehran 1991943344, Iran.
Email: hsazgar@email.kntu.ac.ir

Trajectory planning

Real-time trajectory planning has different aspects such as the geometric curve/approach, collision avoidance, vehicle operating range, vehicle dynamics and computational cost. Recently, Katrakazas et al.[5] conducted a comprehensive and perfect survey on motion planning. One of the important issues that has received less attention is vehicle capability in critical driving situations. Some studies focused on constant speed driving.[6,7] Most researchers have considered only kinematic constraints.[8–10] In some studies, the vehicle behaviour has been approximated as a linear dynamic model.[11–13] Many authors have assumed that maximum longitudinal or/and lateral acceleration is/are limited.[14,15] Jeong hwan et al.[16] proposed an RRT* optimal motion planning algorithm based on nonlinear vehicle and tyre dynamics. In Altché et al.,[17,18] a simulation-based approach offered to compute synthetic feasibility envelopes for the vehicle. These envelopes can be used in motion planning. However, when friction changes, this method will not be so effective.

One of the most common curves that has been utilized for lane change manoeuvres is polynomial.[8,19] The popularity of polynomial curves is due to their continuity and simplicity. In Samiee et al.,[6] a five-degree polynomial is used for lane change manoeuvres. Also, the proposed algorithm generates collision-free and dynamically feasible trajectories. However, this study has some limitations. The most important restriction is the constant speed of the host vehicle (HV). Besides, to find the final manoeuvre time, several high nonlinear equations must be solved simultaneously. In real-time implementations, this feature causes some problems.

Combined control design

In critical manoeuvres, integrated control of longitudinal and lateral dynamics is inevitable. In previous studies, various control methods have been proposed to solve this interesting problem. Recently, Dixit et al.[20] presented a good survey on trajectory planning and tracking for autonomous overtaking. Some authors use vehicle kinematic model for control analysis.[21–23] Major researches utilize a linear dynamic model.[24–30] Some researchers studied integrated longitudinal and lateral controls only in collision avoidance manoeuvres.[31–33] Therefore, the methods provided by these references cannot be used for all driving manoeuvres. One of the most common techniques in combined control is Model Predictive Control (MPC).[34,35]As a matter of fact, thanks to its capabilities, the MPC manages professionally multi-objective control problems for nonlinear and uncertain systems. However, with increasing dynamic model order, nonlinear terms and constraints, the computational burden became greater.

Contributions

One of the most common manoeuvres that is difficult even for experienced drivers is critical high-speed lane change. In this manoeuvre, both vehicle dynamic and tyre dynamic are highly nonlinear. On the contrary, factors such as short manoeuvre duration, limited vehicle dynamic capability, restricted tyre dynamic capacity and no collision with adjacent vehicles make driving more difficult. This paper presents a combined longitudinal and lateral guidance system including trajectory planning and integrated control for these manoeuvres. The proposed trajectory planning method can produce collision-free and feasible trajectories. The integrated control has a good tracking performance and guaranties vehicle stability. Moreover, it covers uncertainties including tyre dynamics and driveline dynamics. Also, both trajectory planning and control method have low computational cost. The significant feature of this control algorithm is that longitudinal control and lateral control are designed based on the desired longitudinal position and desired lateral position, respectively. This feature is extremely important for collision avoidance. In fact, at the moment of passing two vehicles side by side, there must be a safe distance between them. Assuming that the position of the target vehicle (TV) is known at the moment, in order to maintain a safe distance, the HV's position must be controlled. In most integrated control methods, longitudinal control is designed based on the desired longitudinal velocity. Therefore, these methods are not able to control the desired longitudinal position.

The rest of the paper is structured as follows. In the next section, the integrated guidance system is introduced. The 'Vehicle models' section presents the details of the dynamic models used for simulation, control strategy and reference generation. Then, the proposed trajectory planning method and the integrated control algorithm are described. Simulation results and discussion are given in the next section. Finally, the conclusions are presented.

Integrated longitudinal and lateral guidance system

The general architecture of a longitudinal and lateral guidance system was shown in Figure 1. This system has several layers, but we focus on trajectory generation and control. Indeed, we assume that the necessary information from the other layers is completely available. The proposed algorithm can be described as follows: first, considering the TV's position, vehicle dynamics and tyre dynamics, the reference trajectory (X_r, Y_r) was generated. Then, the integrated controller determines the brake/throttle and steering inputs required to track the desired trajectory.

A good application for the proposed algorithm is the critical collision avoidance manoeuvre on a highway (Figure 2). Let the HV and the TV be moving at the same lane on the highway. The vehicles speed is high

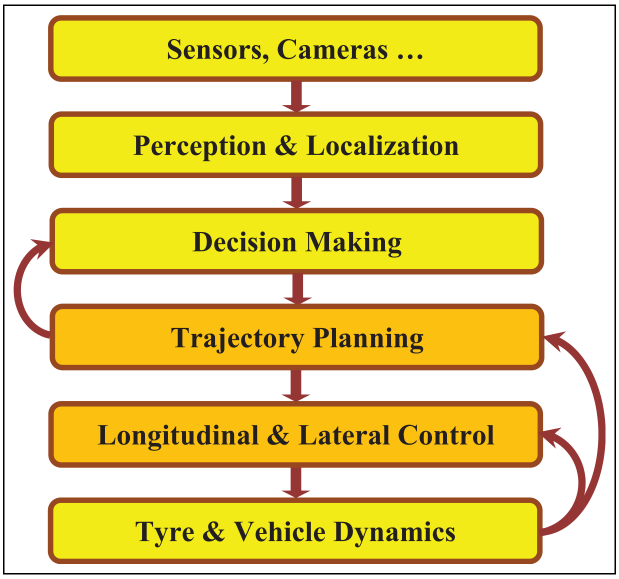

Figure 1. General architecture of a longitudinal and lateral guidance system.

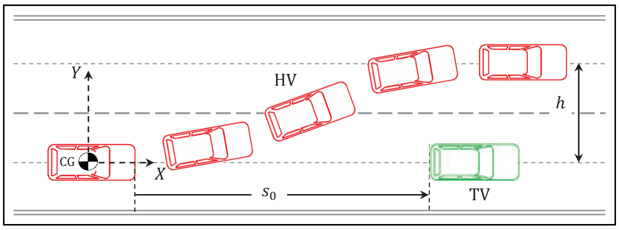

Figure 2. Lane change manoeuvre.

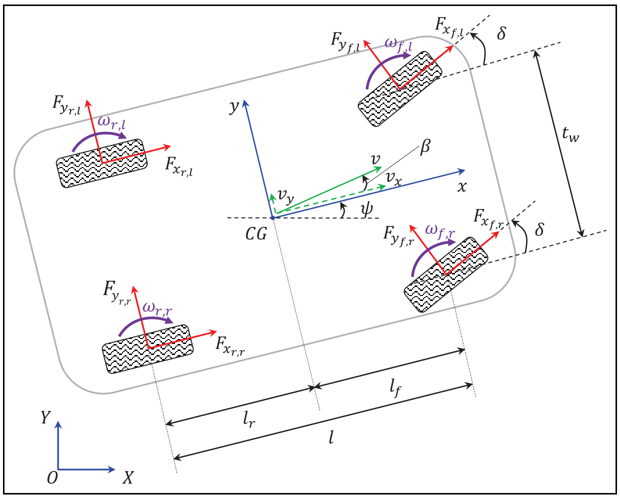

Figure 3. Seven degree of freedom vehicle model.

and the inter-vehicle distance is small. Suddenly, the TV driver brakes heavily. In this situation, if the HV only uses braking, two vehicles will certainly collide. So the HV must initiate braking and steering simultaneously. It is assumed that the vehicles' initial speed and initial distance between the two vehicles are such that there is at least one possible manoeuvre. Although this algorithm has been developed for high-speed critical lane changes, the main idea may be used for other manoeuvres.

Vehicle models

In vehicle automated guidance analysis, selecting a proper dynamic model is very significant. Selecting the level of complexity of the dynamic model depends on the actual behaviour of the vehicle in the examined manoeuvre. In preceding research, various dynamic models with different levels of complexity and accuracy according to the physical phenomena captured are utilized. Herein three dynamic models have been used.

Full CarSim dynamic model

To evaluate the performance of the proposed algorithm, a full CarSim dynamic model is utilized. The HV is a D-class Sedan. We do not change default vehicle configuration parameters in the CarSim software.

Dynamic model for controller design

Integrated control is designed based on a seven degree of freedom vehicle dynamic model $(x, y, \psi, \omega_{f,l}, \omega_{f,r}, \omega_{r,r}, \omega_{r,l})$. A schematic view of this model is shown in Figure 3. In calculating the normal tyre forces, longitudinal and lateral load transfer due to accelerations is taken into account. Also, Roll dynamic and the vehicle suspension dynamics are neglected. To capture non-linear tyre behaviour in control design, Bakker et al.'s[36] tyre model with uncertainty is used. The dynamic model is presented in more detail below.

Equation of motions

$$ma_{x_{CG}} = \left[\left(F_{x_{f,l}} + F_{x_{f,r}}\right)\cos\delta - \left(F_{y_{f,l}} + F_{y_{f,r}}\right)\sin\delta + \left(F_{x_{r,l}} + F_{x_{r,r}}\right) - F_{aero}\right] \tag{1}$$

$$ma_{y_{CG}} = \left[\left(F_{x_{f,l}} + F_{x_{f,r}}\right)\sin\delta + \left(F_{y_{f,l}} + F_{y_{f,r}}\right)\cos\delta + \left(F_{y_{r,l}} + F_{y_{r,r}}\right)\right] \tag{2}$$

$$I_z\ddot{\psi} = l_f\left[\left(F_{x_{f,l}} + F_{x_{f,r}}\right)\sin\delta + \left(F_{y_{f,l}} + F_{y_{f,r}}\right)\cos\delta\right] - l_r\left(F_{y_{r,l}} + F_{y_{r,r}}\right) \tag{3}$$

where F_{aero} is defined as[37]

$$F_{aero} = \frac{1}{2}\rho C_d A_F (v_x + v_{wind})^2 \tag{4}$$

In equation (4), A_F is considered[37] as $1.6 + 0.00056(m - 765)$. The longitudinal and lateral accelerations of CG (vehicle's centre of gravity) can be represented as

$$a_{xCG} = \dot{v}_x - v_y\dot{\psi} \tag{5}$$

$$a_{yCG} = \dot{v}_y + v_x\dot{\psi} \tag{6}$$

Normal tyre forces

$$F_{z_{f,l}} = m\left[\frac{gl_r - a_{x_{cg}}h_{cg} - \frac{F_{aero}h_{aero}}{m}}{2l} - \frac{l_r}{l}\frac{h_{cg}}{t_w}a_{y_{cg}}\right] \tag{7}$$

$$F_{z_{f,r}} = m\left[\frac{gl_r - a_{x_{cg}}h_{cg} - \frac{F_{aero}h_{aero}}{m}}{2l} + \frac{l_r}{l}\frac{h_{cg}}{t_w}a_{y_{cg}}\right] \tag{8}$$

$$F_{z_{r,l}} = m\left[\frac{gl_f + a_{x_{cg}}h_{cg} + \frac{F_{aero}h_{aero}}{m}}{2l} - \frac{l_f}{l}\frac{h_{cg}}{t_w}a_{y_{cg}}\right] \tag{9}$$

$$F_{z_{r,r}} = m\left[\frac{gl_f + a_{x_{cg}}h_{cg} + \frac{F_{aero}h_{aero}}{m}}{2l} + \frac{l_f}{l}\frac{h_{cg}}{t_w}a_{y_{cg}}\right] \tag{10}$$

Wheel dynamics

$$I_w\dot{\omega}_{\tau,\varepsilon} = -F_{x_{\tau,\varepsilon}}.r_{eff} + (T_d + T_b)_{\tau,\varepsilon} - T_{R_{\tau,\varepsilon}}, \tau \in \{f, r\}, \varepsilon \in \{l, r\} \tag{11}$$

$$T_{R_{\tau,\varepsilon}} = f_r.F_{z_{\tau,\varepsilon}}.r_{eff} \tag{12}$$

Assuming the vehicle is front-wheel drive (FWD)

$$T_{d_{f,l}} = T_{d_{f,r}} = \frac{T_d}{2} \tag{13}$$

The relation between the braking torque applied to each wheel and the total braking torque is given by

$$T_{b_{\tau,l}} = T_{b_{\tau,r}} = \frac{T_{b_\tau}}{2} = \frac{F_{z_\tau}}{F_{z_t}}T_b, \tau \in \{f, r\} \tag{14}$$

Driveline dynamics. In high-speed manoeuvres, it can be assumed that the torque converter is locked. Hence

$$T_e = \frac{T_d}{k_d}, k_d = \eta_d k_{diff} n_g \tag{15}$$

$$\alpha_{th} = f(\omega_e, T_e) \tag{16}$$

where $f(\omega_e, T_e)$ represents the engine map.

Braking dynamics

$$\frac{T_b(s)}{P_b(s)} = \frac{k_b}{\tau_b s + 1} \tag{17}$$

Tyre model

$$F_{\gamma_{\tau,\varepsilon}} = \frac{s_{\gamma_{\tau,\varepsilon}}}{s_{\tau,\varepsilon}}\mu_{\tau,\varepsilon}F_{z_{\tau,\varepsilon}}, \gamma \in \{x, y\}, \tau \in \{f, r\}, \varepsilon \in \{l, r\} \tag{18}$$

$$\mu_{\tau,\varepsilon} = D\sin[C\arctan(Bs_{\tau,\varepsilon})], \tau \in \{f, r\}, \varepsilon \in \{l, r\} \tag{19}$$

$$s_{\tau,\varepsilon} = \sqrt{\left(s_{x_{\tau,\varepsilon}}\right)^2 + \left(s_{y_{\tau,\varepsilon}}\right)^2}, \tau \in \{f, r\}, \varepsilon \in \{l, r\} \tag{20}$$

where B, C and D are constants.[36] These coefficients are based on the default CarSim tyre model and are determined by performing different simulations. The maximum friction coefficient is also assumed to be 0.5.

Longitudinal slip

$$s_{x_{\tau,\varepsilon}} = \frac{v_{rw_{\tau,\varepsilon}} - v_{cw_{\tau,\varepsilon}}}{\max\left(v_{rw_{\tau,\varepsilon}}, v_{cw_{\tau,\varepsilon}}\right)}, \tau \in \{f, r\}, \varepsilon \in \{l, r\} \tag{21}$$

Wheel ground contact point velocity

$$v_{cw_{f,l}} = v_{cg} - \dot{\psi}\left(\frac{t_w}{2} - l_f\beta\right) \tag{22}$$

$$v_{cw_{f,r}} = v_{cg} + \dot{\psi}\left(\frac{t_w}{2} + l_f\beta\right) \tag{23}$$

$$v_{cw_{r,l}} = v_{cg} - \dot{\psi}\left(\frac{t_w}{2} + l_r\beta\right) \tag{24}$$

$$v_{cw_{r,r}} = v_{cg} + \dot{\psi}\left(\frac{t_w}{2} - l_r\beta\right) \tag{25}$$

Rotational equivalent wheel velocity

$$v_{rw_{\tau,\varepsilon}} = r_{eff}\omega_{\tau,\varepsilon}, \tau \in \{f, r\}, \varepsilon \in \{l, r\} \tag{26}$$

Lateral slip

$$s_{y_\tau} \approx \alpha_\tau, \tau \in \{f, r\} \tag{27}$$

Tyre slip angle

$$\alpha_f = \delta - \tan^{-1}\left(\frac{v_y + \dot{\psi}l_f}{v_x}\right) \tag{28}$$

$$\alpha_r = -\tan^{-1}\left(\frac{v_y - \dot{\psi}l_r}{v_x}\right) \tag{29}$$

The vehicle parameters are shown in Table 1.

Dynamic model for trajectory generation

Trajectory planning is conducted based on a bicycle dynamical model (x, y and ψ). Moreover, tyre friction force capacity and dynamic of brake/throttle actuator are considered

$$ma_{x_{cg}} = F_{x_f} + F_{x_r} - F_{aero} \tag{30}$$

$$ma_{y_{cg}} = F_{y_f} + F_{y_r} \tag{31}$$

$$I_z\ddot{\psi} = l_fF_{y_f} - l_rF_{y_r} \tag{32}$$

Trajectory planning

The proposed trajectory generation has two steps. At first, considering collision avoidance criteria for each acceleration value, a trajectory can be achieved. Then, taking into account the vehicle and tyre dynamics, the maximum required friction in each trajectory is determined. Every trajectory whose maximum required friction is more than the available friction will be unacceptable. In the end, the trajectory whose

Table 1. Vehicle parameters of the CarSim D-class, Sedan.

Symbol	Value	Unit	Symbol	Value	Unit
m	1530	kg	k_b	700	(N m)/MPa
I_z	2315	kg m^2	τ_b	0.06	–
l_f	1.11	m	η_d	0.85	–
l_r	1.67	m	k_{diff}	4.1	–
b_f	2.18	m	r_{eff}	0.3	m
b_r	2.74	m	I_w	0.9	kg m^2
w_{HV}	0.85	m	f_r	0.015	–
t_w	1.55	m	B	25	–
h_{CG}	0.52	m	C	1.5	–
h_{aero}	1.39	m	D	0.5	–

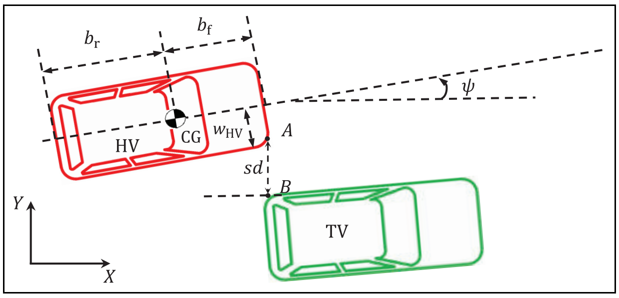

Figure 4. Description of the lateral distance between the HV and the TV.

maximum required friction is lower than the others is chosen as the most appropriate trajectory. The main assumptions used in the development of the trajectory planning method are as follows:

Assumption 1. The vehicle heading remains tangential to the desired trajectory.
Assumption 2. Due to the high speed and short duration of manoeuvre, to maintain vehicle stability, the side angle (ψ) must be small.

Collision avoidance approach

The trajectory collision avoidance algorithm must generate a trajectory which takes into account the geometry of the TV and the HV capabilities. Although geometrically, there are numerous trajectories, all of them are not dynamically feasible. This is discussed in the next section. As shown in Figure 4, during the lane change, the right front corner of the HV (point A) will touch the left rear corner of the TV (point B) if sd be equal to zero. The coordinates of the point B in inertial coordinates are $X_B(t)$ and $Y_B(t)$. We assume that the functions of $X_B(t)$ and $Y_B(t)$ during the manoeuvre are available before trajectory planning. The desired lateral CG's position ($Y_R(t)$) is considered as a five-degree polynomial. Our motivations for choosing a five-degree polynomial (and no higher degrees) are as follows: It can be twice differentiated so the trajectory is smooth. Furthermore, it only needs two points to generate the trajectory. Then, the desired lateral CG's position in terms of time is given by

$$Y_R(t) = b_1t^5 + b_2t^4 + b_3t^3 + b_4t^2 + b_5t + b_6 \tag{33}$$

where b_1 to b_6 are coefficients of the polynomial which can be calculated by applying boundary conditions to the above equation. Herein, it is assumed that at the beginning of the manoeuvre, the CG coincides with the origin of the inertia coordinates axes. In addition, the acceleration and lateral velocity of the HV at the beginning and end of the lane change are zero. The lateral displacement of the HV at the end of the manoeuvre is h. Also, t_f represents the lane change duration that is unknown now.

By applying these boundary conditions to equation (33), $Y_R(t)$ is obtained as

$$Y_R(t) = \left(\frac{6h}{t_f^5}\right)t^5 - \left(\frac{15h}{t_f^4}\right)t^4 + \left(\frac{10h}{t_f^3}\right)t^3 \tag{34}$$

The longitudinal motion of the host and TVs can be arbitrary. However, in order to complete the formulation of the proposed method, it is assumed that the HV and the TV travel at constant accelerations a_{HV} and a_{TV}, respectively. To consider the dynamic of brake/throttle actuator in trajectory generation, the desired longitudinal acceleration defined as a step response of a first-order transfer function with the time constant $1/K$. According to Figure 4 and assumption 1, the reference longitudinal position of points A and B are represented as

$$X_A(t) = a_{HV}\left[\frac{1}{K^2}\left(1 - e^{-Kt}\right) - \frac{t}{K} + \frac{t^2}{2}\right] + v_0t + b_f \tag{35}$$

$$X_B(t) = \frac{1}{2}a_{TV}t^2 + v_0t + \left(s_0 + b_f\right) \tag{36}$$

We assume that at $t = t_c, X_A = X_B$ (Figure 4). By equating the right-hand sides of equations (35) and (36), t_c and then $Y_B(t_c)$ are determined. According to Figure 4, the lateral positions of points A and B at t_c can be written as

$$Y_A(t_c) = Y_B(t_c) + sd \tag{37}$$

where $Y_A(t_c)$ is given by

$$Y_A(t_c) = Y_R(t_c) - w_{HW}\cos\psi_R(t_c) + b_f\sin\psi_R(t_c) \tag{38}$$

where ψ_R is the reference vehicle yaw angle. $\dot{Y}_R(t_c)$ and $v_R(t_c)$ are known, so ($\psi_R(t_c)$) can be determined. Under assumption 1, equation (38) can be rewritten as

$$Y_A(t_c) = Y_R(t_c) - w_{HV} + b_f\frac{\dot{Y}_R(t_c)}{v_R(t_c)} \tag{39}$$

Substituting $Y_A(t_c)$ in equation (37) and after simplification, the following five-degree polynomial equation turns out

$$t_f^5 - 10ht_c^2\left(t_c + \frac{3b_f}{v_R(t_c)}\right)t_f^2 + 15ht_c^3\left(t_c + \frac{4b_f}{v_R(t_c)}\right)t_f - 6ht_c^4\left(t_c + \frac{5b_f}{v_R(t_c)}\right) = 0 \tag{40}$$

where t_f is unknown. By solving the above equation, t_f is obtained and the trajectory is quite determined. It is obvious that for different values of a_{HV}, different trajectories will be generated.

Dynamic feasibility analysis

The evaluation of dynamic feasibility is a very complicated problem because both the vehicle dynamics and tyre dynamics should be taken into account. The objective of this section is to provide a new algebraic approach for dynamic feasibility analysis of critical high-speed manoeuvres. Indeed, in this method, there is no need to solve differential equations (including wheel dynamics, vehicle motion and controller equations). This analysis is based on the tyre–road friction capacity. In fact, if the tyre–road interface cannot provide the required friction for a trajectory, the trajectory will not be feasible, and vice versa. If the required friction coefficient is closer to the maximum available friction coefficient, the trajectory will be more critical. At the end of the collision avoidance section, the free collision trajectories are determined. So for each trajectory a_{xR}, a_{yR}, $\dot{\psi}_R$ and $\ddot{\psi}_R$ in terms of time are known. By substituting these values into equations (7)–(10), normal tyre forces are found. According to equations (11), (13) and (14), by replacing $(a_{xCG})_R$ in equation (30), the longitudinal tyre forces can be written as

$$F_{x_\tau} = \frac{F_{z_\tau}}{mg}(ma_{xR} + F_{aero}), \tau \in \{f, r\} \tag{41}$$

during braking and

$$F_{x_f} = (ma_{xR} + F_{aero}), F_{x_r} = 0 \tag{42}$$

during traction.

Also, substituting $(a_{y_{CG}})_R$ and $\ddot{\psi}_R$ in (31) and (32) and combining the resulting equations, the lateral tyre forces are obtained as

$$F_{y_f} = \frac{ml_r a_{yR} + I_z\ddot{\psi}_R}{l} \tag{43}$$

$$F_{y_r} = \frac{ml_f a_{yR} - I_z\ddot{\psi}_R}{l} \tag{44}$$

Now, the average friction coefficient of the front/rear tyres and the maximum required friction coefficient ($\mu_{req,max}$) during the manoeuvre can be calculated.

Table 2. Details of the collision avoidance manoeuvres.

Symbol	Value	Unit
v_0	80	km/h
v_{wind}	0	km/h
s_0	5	m
h	4	m
a_{HV}	0, –2, –2.5, –4	m/s^2
a_{TV}	–8	m/s^2
w_{TV}	0.85	m
sd	0.6	m
$\mu_{ro,max}$	0.50	–

$$\mu_{req,max} = \max\left(\frac{\sqrt{F_{x_f}^2 + F_{y_f}^2}}{F_{z_f}}, \frac{\sqrt{F_{x_r}^2 + F_{y_r}^2}}{F_{z_r}}\right) \tag{45}$$

If at least at one point of trajectory, $\mu_{req,max}$ is greater than the maximum available frictional coefficient ($\mu_{ro,max}$), then the trajectory will not be dynamically feasible. In order to choose the most appropriate trajectory among all collision-free trajectories, $\mu_{req,max}$ must be calculated for all trajectories. Finally, the trajectory that $\mu_{req,max} < \mu_{ro,max}$ and has the smallest $\mu_{req,max}$ will be the most appropriate one.

Herein, the question may arise whether this criterion, maximum required friction coefficient, is sufficient to choose the most appropriate trajectory. In general, there are different criteria such as collision avoidance, vehicle stability, passenger comfort and fuel consumption for choosing the most appropriate trajectory. However, in critical manoeuvres, these criteria may change. In these manoeuvres, collision free and vehicle stability are the priorities and the other criteria are not so important. In this study, the collision avoidance condition is assumed to be the same for all trajectories. Therefore, the trajectory that provides more vehicle stability margins would be the most appropriate one. According to equation (19), by increasing the friction coefficient, the total tyre slip is increased. The higher tyre slip would lead to higher side slip angle. When the side slip angle increases, the yaw stability margin is decreased. Finally, it can be concluded that maximum required friction coefficient criterion is sufficient.

Trajectory planning results

To investigate the proposed trajectory planning method, a critical collision avoidance manoeuvre is considered. The overview of the critical collision avoidance manoeuvre was presented in the 'Integrated longitudinal and lateral guidance system' section. Its specifications are summarized in Table 2. It is assumed that the TV's acceleration and the lateral position of the B point (w_{TV}) are constant during the manoeuvre.

It is assumed that the collision avoidance scenario is conducted with four different accelerations. By

Table 3. Specification of collision free trajectories.

Trajectory no.	a_{HV}	t_c	t_f	$\mu_{req,max}$	
	(m/s^2)	(s)	(s)	Front tyres	Rear tyres
1	0	1.11	2.17	0.51	0.50
2	–2	1.26	2.47	0.43	0.48
3	–2.5	1.31	2.56	0.43	0.48
4	–4	1.51	2.96	0.48	0.53

replacing the manoeuvre data from Table 2 in the equations of the 'Collision avoidance approach' section, for each acceleration, a trajectory is obtained. Once the trajectory's specifications are determined, using the method presented in section 'Dynamic feasibility', the maximum required friction in each trajectory can be determined. The summary of the results is given in Table 3.

When the longitudinal acceleration is zero, the required longitudinal forces are negligible. However, because of the short manoeuvre duration (relative to other trajectories), the lateral acceleration is high. Therefore, the resulting required lateral tyre forces will be large. This results in the maximum required friction coefficient to be 0.51. On trajectory 2, by applying brake, the necessary longitudinal tyre force is more than the previous one. Also, by increasing manoeuvre time (from 2.17 to 2.47 s), the maximum lateral acceleration declines. As a result, required lateral tyre forces are lower. This increasing and decreasing make the maximum necessary tyre forces go down; therefore, the maximum required friction coefficient drops from 0.51 to 0.48. By rising the deceleration to 2.5m/s^2, an interesting event occurs. Although the deceleration is more than deceleration of trajectory 2, the maximum required friction coefficient remains almost constant. The cause of this happening can be described as follows: compared to trajectory 2, the increasing of the longitudinal tyre force is almost equal to the reduction of lateral forces; so the maximum required friction stays at the same level. It is expected that further deceleration makes the maximum friction to increase. By evaluating the results of trajectory 4, the correctness of this statement is well proved. According to the aforementioned results, based on the minimum required friction criterion, trajectories 2 and 3 with a maximum friction coefficient of 0.48 are the most appropriate trajectories. It will be shown in section 'Evaluation of the trajectory planning method' that simulation results of the close loop system confirms the results obtained from the trajectory planning method.

Combined longitudinal and lateral control

In this section, using the sliding mode control approach,[38] an integrated controller will be developed. This control algorithm simultaneously ensures good longitudinal and lateral position tracking. In the longitudinal control, the two inputs considered for traction and braking modes are brake master cylinder pressure and throttle opening, respectively. In addition, the vehicle lateral dynamic is controlled by the front-wheel steering angle.

Longitudinal control

The longitudinal control aims to track the reference longitudinal position generated by the trajectory planning system. To use the sliding mode approach presented in Slotine,[38] a relation between the longitudinal position (or one of its derivatives) with the torques applied to the wheels should be extracted. Assuming $X(t) = \int_0^t (v_x \cos\psi - v_y \sin\psi)dt$ and X_R are reference longitudinal position and vehicle longitudinal position, the error of the longitudinal position can be defined as $e_X = X - X_R$. The sliding surface for longitudinal control is written as follows

$$ss_x = \left(\frac{d}{dt} + \lambda_x\right)^1 e_X \tag{46}$$

Differentiating ss_x

$$\dot{ss}_x = [\dot{v}_x \cos\psi - N\cos\psi] \tag{47}$$

where

$$N = \frac{v_x\dot{\psi}\sin\psi + \dot{v}_y\sin\psi + \ddot{X}_r + \lambda_x\left(v_y\sin\psi + \dot{X}_R\right)}{\cos\psi} - \lambda_x v_x + v_y\dot{\psi}$$

Assuming $\dot{ss}_x = 0$, $\dot{v}_x$ is achieved

$$\dot{v}_x = N \tag{48}$$

Also, using longitudinal dynamic, $\dot{v}_x$ can be obtained as (49) and (50) for braking and traction mode, respectively

$$\dot{v}_x = \frac{1}{m}\left[\frac{T_b}{r_{eff}} - \frac{f_r r_{eff} F_{zf} + I_w\left(\dot{\omega}_{f,l} + \dot{\omega}_{f,r}\right)}{r_{eff}}\cos\bar{\delta} - \left(f_r r_{eff} F_{zr} + \frac{I_w}{r_{eff}}(\dot{\omega}_{r,l} + \dot{\omega}_{r,r})\right) - \overline{F_{y_f}}\sin\bar{\delta} - F_{aero}\right] + v_y\dot{\psi} \tag{49}$$

$$\dot{v}_x = \frac{1}{m}\left[\frac{T_d}{r_{eff}} - \left(\frac{f_r r_{eff} F_{zf} + I_w\left(\dot{\omega}_{f,l} + \dot{\omega}_{f,r}\right)}{r_{eff}}\right)\cos\bar{\delta} - \overline{F_{y_f}}\sin\bar{\delta} - F_{aero}\right] + v_y\dot{\psi} \tag{50}$$

By equating the right-hand sides of equations (48) and (49), the total equivalent braking torque is obtained

$$T_{b_{eq}} = r_{eff}\left[f_r\hat{F}_{zf}\cos\bar{\delta} + f_r\hat{F}_{zr} + \hat{\overline{F}}_{y_f}\sin\bar{\delta} + \hat{F}_{aero} - mv_y\dot{\psi} + mN\right] + I_w\left(\left[\dot{\omega}_{f,l} + \dot{\omega}_{f,r}\right]\cos\bar{\delta} + \dot{\omega}_{r,l} + \dot{\omega}_{r,r}\right) \tag{51}$$

In addition, by equating the right-hand sides of equations (48) and (50), the equivalent engine torque is achieved

$$T_{e_{eq}} = \hat{k}_d\Big[r_{eff}\Big(f_r\hat{F}_{zf}\cos\bar{\delta} + \hat{\bar{F}}_{y_f}\sin\bar{\delta} + \hat{F}_{aero} - mv_y\dot{\psi} + mN\Big) + I_w\left(\dot{\omega}_{f,l} + \dot{\omega}_{f,r}\right)\cos\bar{\delta}\Big] \tag{52}$$

According to Slotine,[38] the sliding condition can be written as

$$ss_x\dot{s}s_x \leqslant -\eta_x|ss_x| \tag{53}$$

By substituting $\dot{s}s_x$ from (47) into (53)

$$ss_x[\dot{v}_x\cos\psi - N\cos\psi] \leqslant -\eta_x|ss_x| \tag{54}$$

In order to satisfy sliding condition (54) despite uncertainty on the vehicle and tyre dynamics, a term must be added to T_{eq}.

Since the braking and the driveline dynamics are completely independent of each other, the remainder of the longitudinal control design will be made separately for each one.

Braking mode. By replacing $\dot{v}_x$ from (49) into (54) and multiplying both sides of the resulting inequality by $mr_{eff}/\cos\psi$

$$\begin{aligned} &ss_x\Big\{T_b - f_r r_{eff}\big(F_{zf}\cos\bar{\delta} + F_{zr}\big) - I_w\left(\dot{\omega}_{f,l} + \dot{\omega}_{f,r}\right)\cos\bar{\delta} \\ &+ I_w\left(\dot{\omega}_{rf,l} + \dot{\omega}_{r,r}\right) - r_{eff}\bar{F}_{y_f}\sin\bar{\delta} - r_{eff}F_{aero} \\ &+ mr_{eff}v_y\dot{\psi} - mr_{eff}N\Big\} \leqslant -\frac{mr_{eff}\eta_x}{\cos\psi}|ss_x| \end{aligned} \tag{55}$$

by considering total braking torque as $T_b = T_{b_{eq}} - k_{x,b}\mathrm{sat}(ss_x, \varnothing_x)$ and substituting it in (55), inequality (55) can be rewritten as

$$\begin{aligned} &ss_x\Big\{f_r r_{eff}\big[\big(F_{zf}\cos\bar{\delta} + F_{zr}\big) - \big(\hat{F}_{zf}\cos\bar{\delta} + \hat{F}_{zr}\big)\big] \\ &+ r_{eff}\big(F_{aero} - \hat{F}_{aero}\big) + r_{eff}\Big(\bar{F}_{y_f}\sin\bar{\delta} - \hat{\bar{F}}_{y_f}\sin\bar{\delta}\Big)\Big\} \\ &+ \frac{mr_{eff}\eta_x}{\cos\psi}|ss_x| \leqslant k_{x,b}\mathrm{sat}(ss_x, \varnothing_x)ss_x \end{aligned} \tag{56}$$

Defining the following uncertainty bounds

$$\begin{aligned} &\big|f_r r_{eff}\big[\big(F_{zf}\cos\bar{\delta} + F_{zr}\big) - \big(\hat{F}_{zf}\cos\bar{\delta} + \hat{F}_{zr}\big)\big]\big| \\ &\leqslant 0.15 f_r r_{eff}\big(\hat{F}_{zf}\cos\bar{\delta} + \hat{F}_{zr}\big) = U_{roll} \\ &\big|r_{eff}\big(F_{aero} - \hat{F}_{aero}\big)\big| \leqslant 0.15 r_{eff}\hat{F}_{aero} = U_{aero} \\ &\Big|r_{eff}\Big(\bar{F}_{y_f}\sin\bar{\delta} - \hat{\bar{F}}_{y_f}\sin\bar{\delta}\Big)\Big| \leqslant 0.15 r_{eff}\Big|\hat{\bar{F}}_{y_f}\sin\bar{\delta}\Big| = U_{F_{y_f}} \end{aligned}$$

the sliding condition can be written as the following condition

$$U_{roll} + U_{aero} + U_{F_{y_f}} + \frac{mr_{eff}\eta_x}{\cos\psi} \leqslant k_{x,b} \tag{57}$$

Considering an appropriate value for $\varnothing_x$, the total braking torque is achieved. Finally, by using (17), the master cylinder pressure can be determined.

Traction mode. At first, we consider the following uncertainty for the driveline dynamics

$$k_{d,max} = 1.05\eta_d k_{diff} n_g, k_{d,min} = 0.95\eta_d k_{diff} n_g,$$
$$\hat{k}_d = \sqrt{k_{d,max}.k_{d,min}} = 0.85$$

By defining total engine torque as $T_e = T_{e_{eq}} - \hat{k}_d k_{x,t}\mathrm{sat}(ss_x, \varnothing_x)$ and substituting it in (54), sliding condition is given by

$$\begin{aligned} &ss_x\left\{\frac{T_{e_{eq}} - \hat{k}_d k_{x,t}\mathrm{sat}(ss_x, \varnothing_x)}{k_d} - \left[f_r r_{eff}F_{zf} + I_w\left(\dot{\omega}_{f,l} + \dot{\omega}_{f,r}\right)\right]\cos\bar{\delta} - r_{eff}\bar{F}_{y_f}\sin\bar{\delta} - r_{eff}F_{aero} + mr_{eff}v_y\dot{\psi} - mr_{eff}N\right\} \\ &\leqslant -\frac{mr_{eff}\eta_x}{\cos\psi}|ss_x| \end{aligned} \tag{58}$$

Adding and subtracting $T_{e_{eq}}/\hat{k}_d$, the inequality (58) can be rewritten as

$$\begin{aligned} &ss_x\left\{\left(\frac{1}{k_d} - \frac{1}{\hat{k}_d}\right)T_{eq} + \Big(r_{eff}f_r\big[\big(\hat{F}_{zf}\cos\bar{\delta} + \hat{F}_{zr}\big) - \big(F_{zf}\cos\bar{\delta} + F_{zr}\big)\big] + r_{eff}\Big(\hat{\bar{F}}_{y_f}\sin\bar{\delta} - \bar{F}_{y_f}\sin\bar{\delta}\Big) + r_{eff}\big(\hat{F}_{aero} - F_{aero}\big)\Big)\right\} \\ &+ \frac{mr_{eff}\eta_x}{\cos\psi}|ss_x| \leqslant \frac{\hat{k}_d k_{x,t}}{k_d} \end{aligned} \tag{59}$$

By defining $\beta_x = \sqrt{k_{d,max}/k_{d,min}}$ and multiplying both sides of the above inequality by $k_d/\hat{k}_d$, after some simplification, the sliding condition can be written as

$$\begin{aligned} &\left(k_{d,max} - k_{d,min}\right)\left|T_{eq}\right| \\ &+ \beta_x\left[U_{roll} + U_{aero} + U_{F_{y_f}} + \frac{mr_{eff}\eta_x}{\cos\psi}\right] \leqslant k_{x,t} \end{aligned} \tag{60}$$

Considering an adequate value for $\varnothing_x$, the total engine torque is achieved.

Lateral control

Lateral controller steers the vehicle's wheels for reference lateral position tracking. To use the sliding mode strategy introduced in Slotine,[38] a relation between the lateral position (or one of its derivatives) with the steering wheel angle should be found. Combining equations (18), (27) and (28), the front lateral tyre forces are given by

$$F_{y_{f,\varepsilon}} = \left(\delta - \tan^{-1}\left(\frac{v_y + \dot{\psi} l_f}{v_x}\right)\right)\frac{\mu_{f,\varepsilon}}{s_{f,\varepsilon}} F_{z_{f,\varepsilon}} \varepsilon \in \{l, r\} \tag{61}$$

Multiplying both sides of equation (1) by l_r and adding it to equation (3), rear lateral tyre forces are eliminated from the resulting equation. By substituting front lateral tyre forces from (61) in this equation, $\dot{v}_y$ is obtained as

$$\begin{aligned}\dot{v}_y = &\frac{l \sin\delta}{m l_r}\left(F_{x_{f,l}} + F_{x_{f,r}}\right) + b\delta \\ &- b\tan^{-1}\left(\frac{v_y + \dot{\psi} l_f}{v_x}\right) - v_x \dot{\psi} - \frac{I_z}{m l_r}\ddot{\psi}\end{aligned} \tag{62}$$

where

$$b = \frac{l\cos\delta}{m l_r}\left(\frac{\mu_{f,l}}{s_{f,l}} F_{z_{f,l}} + \frac{\mu_{f,r}}{s_{f,r}} F_{z_{f,r}}\right)$$

Assuming $Y(t) = \int_0^t (v_x \sin\psi + v_y \cos\psi) dt$ and Y_R are reference lateral position and vehicle lateral position, the error of the lateral position can be defined as $e_Y = Y - Y_R$. The sliding surface for lateral control is given by

$$ss_y = \left(\frac{d}{dt} + \lambda_y\right)^1 e_Y, \lambda_y > 0 \tag{63}$$

Differentiating ss_y

$$\dot{ss}_y = \left[\dot{v}_y \cos\psi - M\cos\psi\right] \tag{64}$$

where

$$M = \frac{v_y \dot{\psi} \sin\psi - \dot{v}_x \sin\psi + \ddot{Y}_R - \lambda_y\left(v_x \sin\psi - \dot{Y}_r\right)}{\cos\psi} - v_x \dot{\psi} - \lambda_y v_y$$

Assuming $\dot{ss}_y = 0, \dot{v}_y$ is achieved

$$\dot{v}_y = M \tag{65}$$

By equating the right-hand sides of equations (62) and (65), the equivalent wheel steering angle is obtained

$$\begin{aligned}\delta_{eq} = &\frac{1}{\hat{b}}\left[M - \frac{l\sin\bar{\delta}}{m l_r}\left(\hat{F}_{x_{f,l}} + \hat{F}_{x_{f,r}}\right) + \frac{I_z}{m l_r}\ddot{\psi} + v_x\dot{\psi}\right] \\ &+ \tan^{-1}\left(\frac{v_y + \dot{\psi} l_f}{v_x}\right)\end{aligned} \tag{66}$$

According to Slotine,[38] the lateral sliding condition can be written as

$$ss_y \dot{ss}_y \leqslant -\eta_y |ss_y| \tag{67}$$

By substituting $\dot{ss}_y$ from (64) into (67), the above inequality be rewritten as

$$ss_y\left[\dot{v}_y \cos\psi - M\cos\psi\right] \leqslant -\eta_y |ss_y| \tag{68}$$

In order to satisfy sliding condition (67) despite uncertainty on the vehicle and tyre dynamics, a term must be added to δ_{eq}. So the total steering angle is defined as

$$\delta = \delta_{eq} - \frac{k_y sat(ss_y, \varnothing_y)}{\hat{b}} \tag{69}$$

By substituting δ from (69) into (67) and multiplying both sides of resulting equation by $\hat{b}/b$, after some simplification, sliding condition is given by

$$\begin{aligned}&ss_y \cos\psi\left(\left[\frac{\hat{b}}{b}\left[\left(F_{x_{f,l}} - \hat{F}_{x_{f,l}}\right) + \left(F_{x_{f,r}} - \hat{F}_{x_{f,r}}\right)\right] - \left(\hat{F}_{x_{f,l}} + \hat{F}_{x_{f,r}}\right)\left(1 - \frac{\hat{b}}{b}\right)\right]\frac{l\sin\bar{\delta}}{m l_r} + \left(1 - \frac{\hat{b}}{b}\right)\left(v_x\dot{\psi} + \frac{I_z}{m l_r}\ddot{\psi} + M\right)\right) \\ &+ \eta_y \frac{\hat{b}}{b}|ss_y| \leqslant k_y |ss_y|\end{aligned} \tag{70}$$

Defining the following uncertainty bounds

$$b_{max} = 1.1\frac{l\cos\bar{\delta}}{m l_r}\left(\frac{\mu_{f,l}}{s_{f,l}} F_{z_{f,l}} + \frac{\mu_{f,r}}{s_{f,r}} F_{z_{f,r}}\right), b_{min} = 0.85\frac{l\cos\bar{\delta}}{m l_r}\left(\frac{\mu_{f,l}}{s_{f,l}} F_{z_{f,l}} + \frac{\mu_{f,r}}{s_{f,r}} F_{z_{f,r}}\right)$$

$$\hat{b} = \sqrt{b_{max}.b_{min}} = 0.99\frac{l\cos\bar{\delta}}{m l_r}\left(\frac{\mu_{f,l}}{s_{f,l}} F_{z_{f,l}} + \frac{\mu_{f,r}}{s_{f,r}} F_{z_{f,r}}\right), \beta_y = \sqrt{\frac{b_{max}}{b_{min}}} = 1.16$$

$$\left|\left(F_{x_{f,l}} - \hat{F}_{x_{f,l}}\right) + \left(F_{x_{f,r}} - \hat{F}_{x_{f,r}}\right)\frac{l\sin\bar{\delta}\cos\psi}{m l_r}\right| \leqslant U_{F_x} = 0.15\left[\left|s_{xf,l}\frac{\mu_{f,l}}{s_{f,l}} F_{z_{f,l}}\right| + \left|s_{xf,r}\frac{\mu_{f,r}}{s_{f,r}} F_{z_{f,r}}\right|\right]\frac{l|\sin\bar{\delta}|\cos\psi}{m l_r}$$

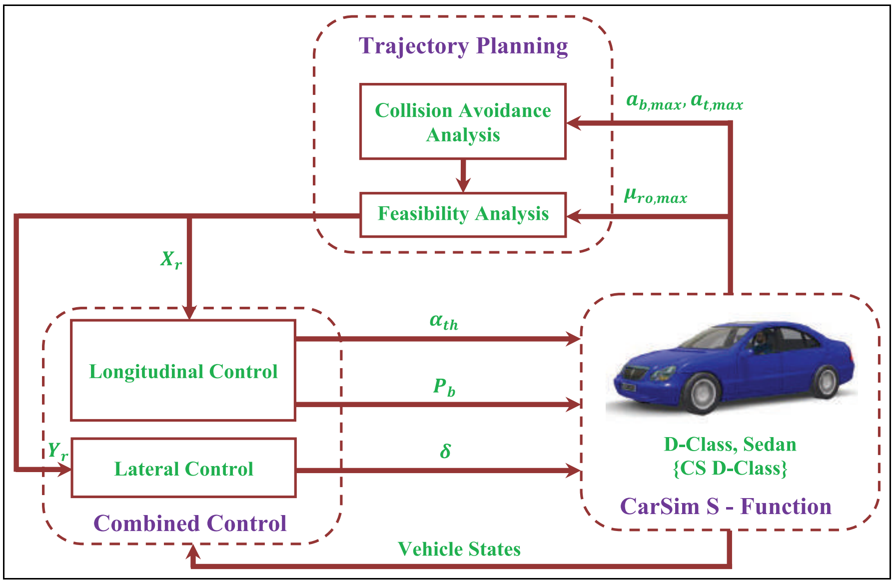

Figure 5. The block diagram of the combined longitudinal and lateral guidance system.

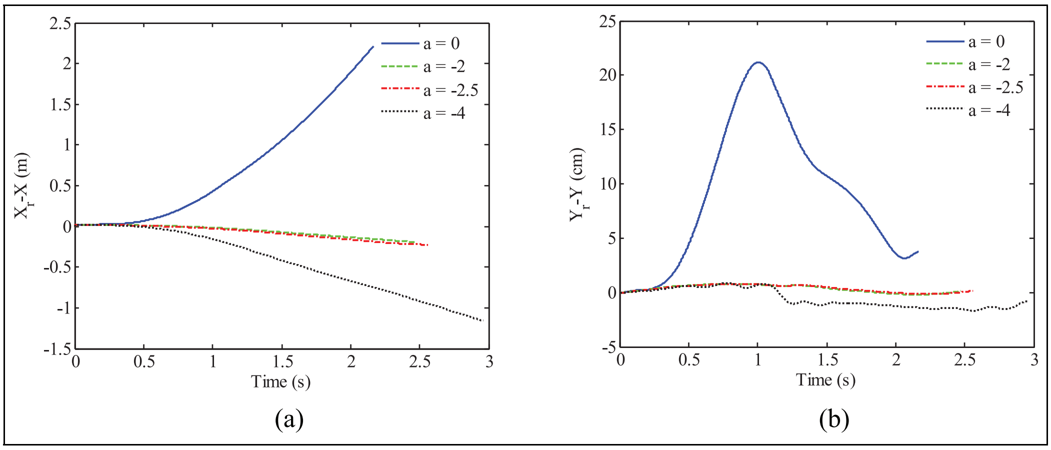

Figure 6. Tracking errors for all trajectories: (a) Longitudinal position error and (b) lateral position error.

Inequality (70) can be rewritten as

$$\left\{\left|\left(\hat{F}_{x_{f,l}}+\hat{F}_{x_{f,r}}\right)\frac{l\cos\psi\sin\bar{\delta}}{ml_r}\right|+\left|v_x\dot{\psi}+\frac{I_z}{ml_r}\ddot{\psi}+M\right|\cos\psi\right\}(\beta_y-1)+\left(U_{F_x}+\eta_y\right)\beta_y\leqslant k_y \quad (71)$$

The lateral sliding condition will be satisfied if k_y is bigger than the left-hand side of the above inequality.

Simulation results and discussion

Simulations are performed using vehicle simulation software, CarSim and MATLAB/Simulink. It should be noted that simulations are performed with the default vehicle configuration parameters in the CarSim software. The block diagram of the combined longitudinal and lateral guidance system is illustrated in Figure 5.

Evaluation of the trajectory planning method

As specified in Table 3, in the first and last trajectories, $\mu_{req,max}$ is bigger than $\mu_{ro,max}$. So, based on the minimum required friction criterion, these trajectories are not dynamically feasible. Herein, an important question may arise; what happens when the HV moves along these trajectories? It is important to note that the friction coefficients in Table 3 are almost equal; so it cannot be said that the vehicle will become necessarily unstable. However, one can certainly expect that with the same controller, the tracking errors of trajectories 2 and 3 are lesser than the others. This issue is well illustrated in Figure 6.

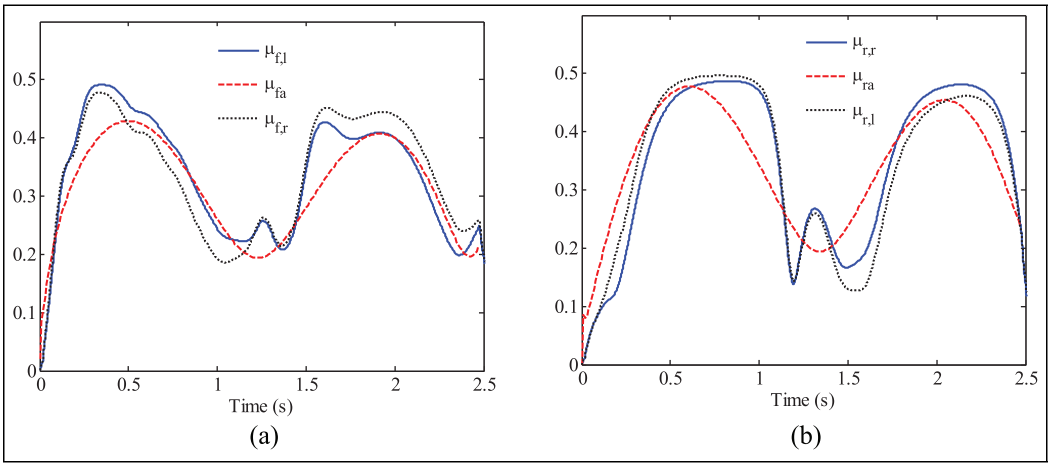

Figure 7. Comparison of approximate average friction coefficients and tyre friction coefficients: (a) Front tyres and (b) rear tyres.

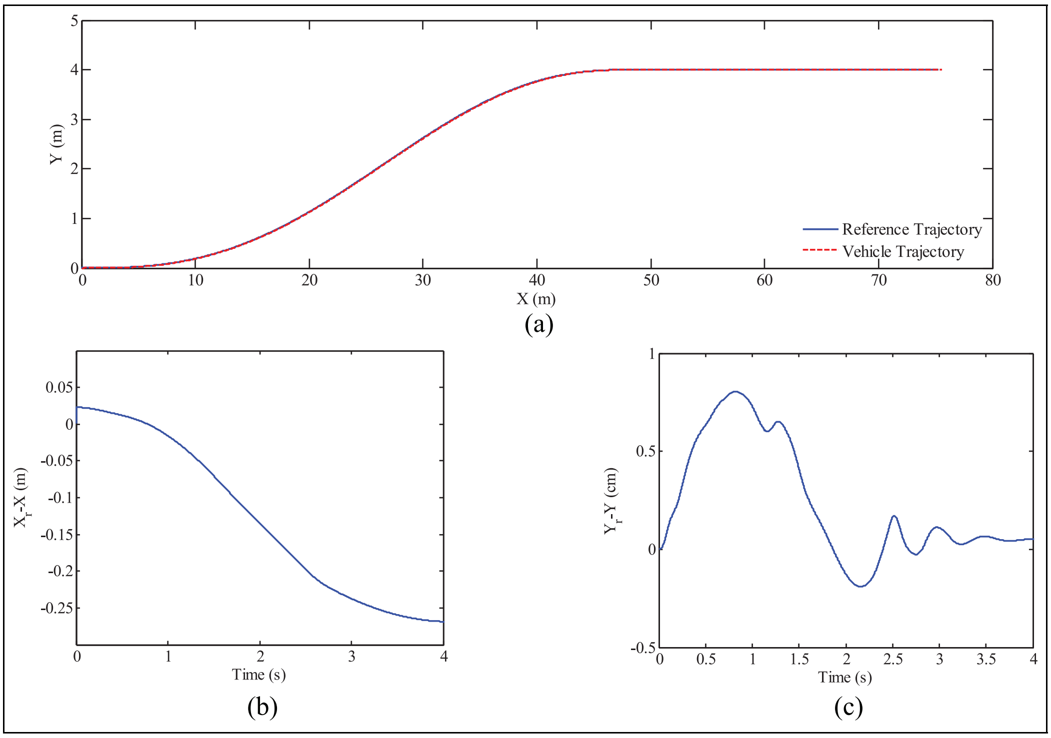

Figure 8. Overall performance of the combined controller: (a) Reference and vehicle trajectories, (b) longitudinal position error and (c) lateral position error.

As noted above, the most appropriate trajectory was selected based on the approximate maximum frictional coefficient of the front and rear tyres. So it is important that the proposed method has sufficient accuracy. For this purpose, the friction coefficients of the tyres and the approximate friction coefficient of the front and rear tyres for trajectory 2 are shown in Figure 7. By comparing the tyre friction coefficients and the average frictional coefficients, it can be concluded that both of them have the same trend. Of course, in the proposed method only the maximum friction coefficient is important. So it is not necessary that the approximate curve coincides with the actual curve! In terms of quantity, the approximate friction coefficients are slightly less than the actual friction coefficients. The difference between the two values is due to the difference between the actual and approximate accelerations. Indeed, in the trajectory planning method, it was assumed that the vehicle heading remains tangential to the desired trajectory. In other words, v_y was assumed to be zero. So, according to equation (5), the approximate longitudinal acceleration is less than the real acceleration. As a result, the tyre longitudinal force and the resulting total friction will be less than the actual values.

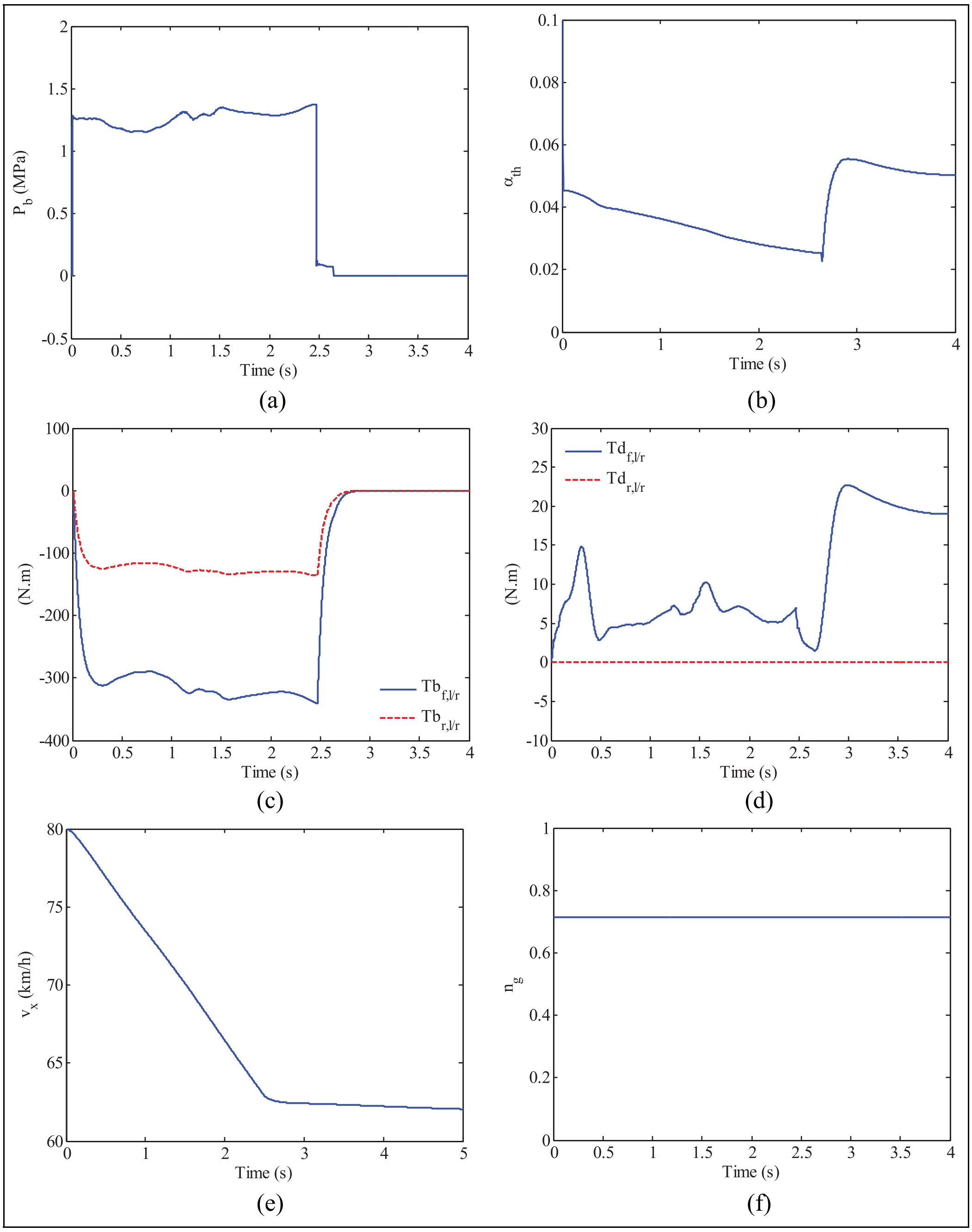

Figure 9. Longitudinal control: (a) Brake master cylinder pressure, (b) throttle opening, (c) wheel braking torques, (d) wheel driving torques, (e) longitudinal speed and (f) transmission gear ratio.

Detailed combined longitudinal and lateral control results

In this section, the integrated control performance for trajectory 2 will be elaborated in detail. It is also assumed that after the lane change, the vehicle continues to move in a straight line until 4 s at a constant speed. The overall performance of the combined controller is shown in Figure 8(a).

According to Figure 8(b), the maximum longitudinal error is about 0.25 m. Furthermore, the maximum lateral position error is less than 1 cm (Figure 8(c)). Regarding the error values, it can be concluded that the proposed control algorithm presents excellent tracking performance.

Figure 9 illustrates the longitudinal control performance. As noted in the trajectory planning section, the desired longitudinal acceleration in both the braking mode and the traction mode was considered as the step response of the first-order transfer function. This definition, in addition to taking into account the dynamics of the throttle and brake actuators, causes that the control inputs do not change suddenly.

As can be seen in Figure 9(a) and (c), change of brake master cylinder pressure and the wheel braking torques are completely continuous and smooth. This feature is also seen in the throttle opening and the wheel driving torques (Figure 9(b) and (d)). As

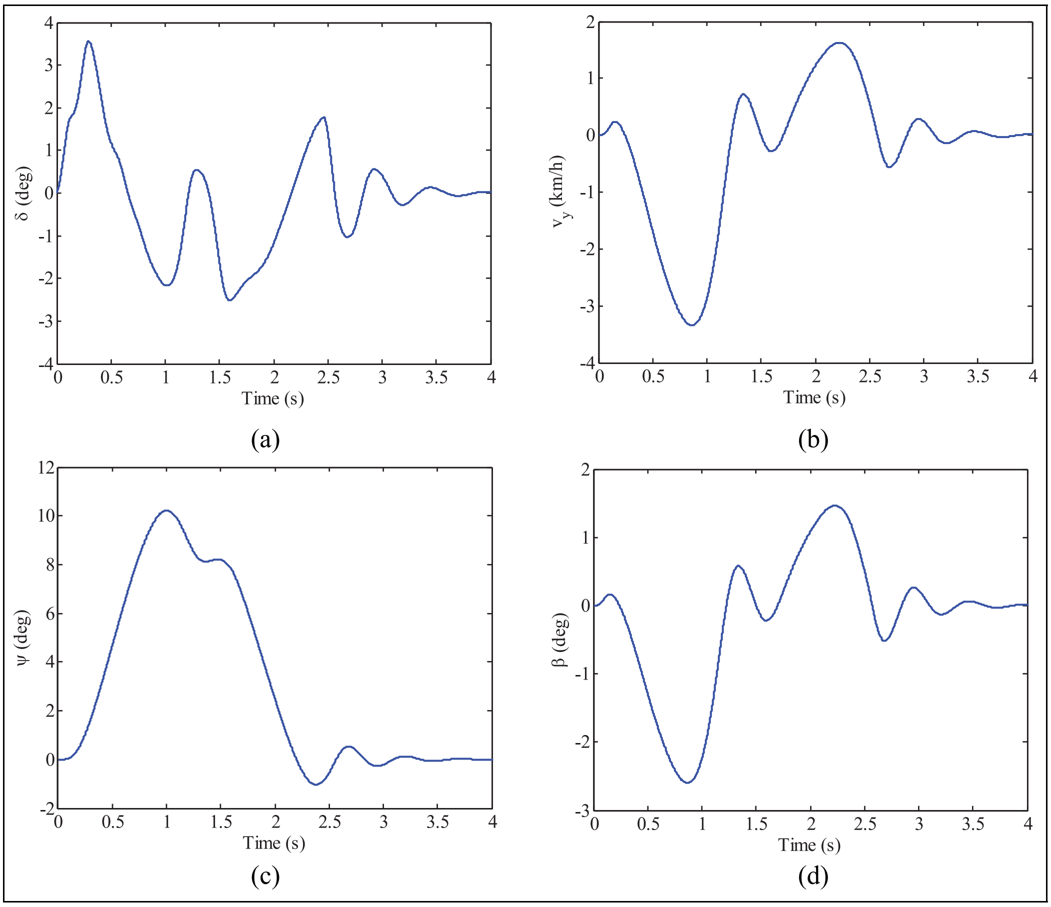

Figure 10. Lateral control: (a) Front-wheel steering angle, (b) lateral speed, (c) heading angle and (d) side-slip angle.

Figure 9(e) indicates, the vehicle speed at the end of the manoeuvre is 62 km/h. Also, during the manoeuvre, the transmission gear ratio remains constant at 0.7 (Figure 9(f)).

The lateral control performance is presented in Figure 10. With respect to Figure 10(a), the steering input angle is perfectly uninterrupted and uniform. For further explanation of the lateral states of the vehicle, lateral speed, heading angle and side-slip angle are shown in Figure 10(b)–(d), respectively. As can be seen in Figure 10(c), the maximum side-slip angle is less than 2.6°. As a result, the correctness of assumption 1 is verified. Besides, the small slip angle ensures yaw stability which is very much worthwhile.

A more complex lane change scenario

In order to better demonstrate the capabilities of the proposed method, a more complex scenario is considered. As shown in Figure 11, this scenario includes three vehicles that are quite similar in size. These vehicles are moving at the same lane on the highway (Figure 11(a)). The initial conditions of the TV and HV1 are exactly the same as the previous scenario (Table 3). It is assumed that the reference trajectory for HV1 is trajectory 2 (Table 3). HV1 starts to lane change to lane 2. After 0.5 s, HV2 decides to overtake HV1 and go to lane 3 (Figure 11(b)). At this moment, the initial speed of HV2 is 90km/h and the longitudinal distance with HV1 is 9.3 m. The positions of the three vehicles at t_c (the moment that HV2 reaches to HV1) and the end of the manoeuvre are shown in Figure 11(c) and (d), respectively. In this scenario, it is assumed that HV1 and HV2 are automated and under the control of a central system. Therefore, HV2 is aware of the reference trajectory of HV1.

This manoeuvre can be performed with different accelerations. However, according to assumptions, if the deceleration is bigger than $2\mathrm{m/s}^2$, the speed of HV2 at the end the manoeuvre will be smaller than the speed of HV1, and overtaking will not be possible. The results of the trajectory planning method for three acceleration (0, –1, –2) are presented in Table 4.

According to Table 4, on trajectories 1, 2 and 3, the maximum required frictions are 0.65, 0.53 and 0.41, respectively. So, based on the minimum required friction criterion, trajectory 3 is the most appropriate trajectory. The control performance for these trajectories also confirms this (Figure 12).

Longitudinal and lateral tracking errors of three trajectories are illustrated in Figure 13(a) and (b), respectively. Comparing the tracking errors and maximum required friction associated with each trajectory, it can

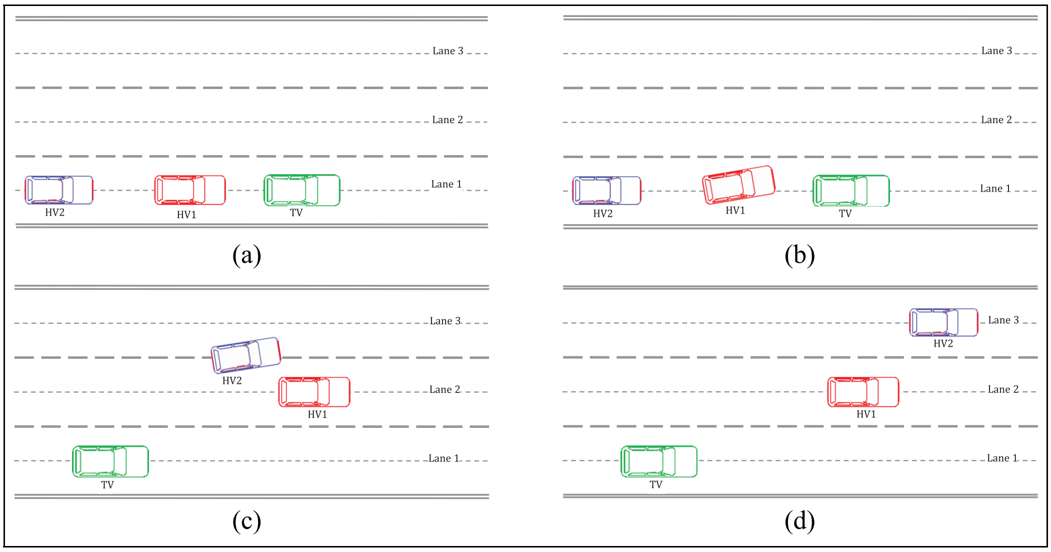

Figure 11. Complex scenario: (a) initial vehicle positions, (b) start of the manoeuvre, (c) moment that HV2 reaches to HV1 and (d) the end of manoeuvre.

Table 4. Results of trajectory planning method for complex scenarios.

Trajectory no.	a_{HV} (m/s^2)	t_c (s)	t_f (s)	$\mu_{req,max}$ Front tyres	Rear tyres
1	0	1.73	2.73	0.65	0.63
2	–1	1.98	3.08	0.51	0.53
3	–2	2.46	3.84	0.37	0.41

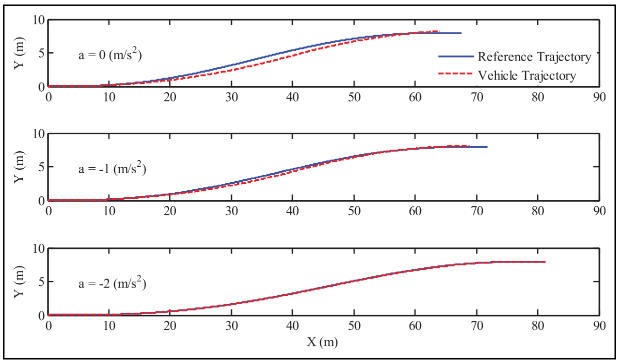

Figure 12. Reference and vehicle trajectories for complex scenario.

be concluded that the proposed trajectory planning method works effectively.

Conclusion

This paper presents an integrated longitudinal and lateral vehicle guidance system for critical high-speed lane change manoeuvres. This algorithm provides suitable solutions to the problem of trajectory planning and tracking control. The simulation results for critical collision avoidance manoeuvres confirmed the effectiveness and high capabilities of the proposed algorithm. The most important features of the proposed algorithm are as follows:

1. In order to be close to the actual behaviour of the vehicle, both in the trajectory planning and in the combined control design, the longitudinal and lateral load transfer, the nonlinear tyre dynamics and the dynamics of throttle and brakes actuators are considered.
2. The proposed algorithm can be reliably used in all critical high-speed lane change manoeuvres including constant speed, braking and acceleration ones.
3. Compared to other studies, as the trajectory planning was performed algebraically, the computational cost is highly low. This is very valuable in real-time implementations.
4. The proposed integrated longitudinal and lateral controller demonstrates an excellent tracking performance and ensures vehicle stability.
5. Combined control was designed based on longitudinal and lateral position errors, so the HV position is fully controlled. This issue is especially important in collision avoidance manoeuvres.

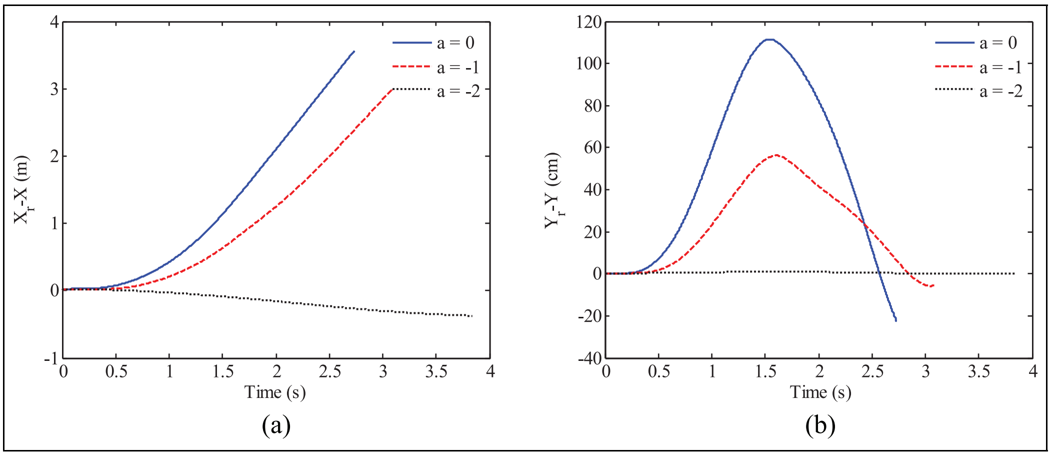

Figure 13. Tracking errors for three trajectories (complex scenario): (a) Longitudinal position error and (b) lateral position error.

Declaration of conflicting interests

The author(s) declared no potential conflicts of interest with respect to the research, authorship and/or publication of this article.

Funding

The author(s) received no financial support for the research, authorship and/or publication of this article.

ORCID iD

Hadi Sazgar https://orcid.org/0000-0002-2208-727X

References

1. World Health Organization. Road traffic injuries, www.who.int/en/news-room/fact-sheets/detail/road-traffic-injuries#content (accessed 21 June 2018).
2. Road Safety. www.roadsafetymayo.ie/CausesofCollisions/ (accessed 21 June 2018).
3. Bengler K, Dietmayer K, Farber B, et al. Three decades of driver assistance systems: review and future perspectives. *IEEE Intell Transp Syst Mag* 2014; 6: 6–22.
4. Ziebinski A, Cupek R, Grzechca D, et al. Review of advanced driver assistance systems (ADAS). *AIP Conf Proc* 2017; 1906: 120002.
5. Katrakazas C, Quddus M, Chen W, et al. Real-time motion planning methods for autonomous on-road driving: state-of-the-art and future research directions. *Trans Res C: Emer* 2015; 60: 416–442.
6. Samiee S, Azadi S, Kazemi R, et al. Towards a decision-making algorithm for automatic lane change maneuver considering traffic dynamics. *PROMET* 2016; 28: 91–103.
7. Wnag C, Zhao W, Xu Z, et al. Path planning and stability control of collision avoidance system based on active front steering. *Sci China Technol Sci* 2017; 60: 1231–1243.
8. You F, Zhang R, Lie G, et al. Trajectory planning and tracking control for autonomous lane change maneuver based on the cooperative vehicle infrastructure system. *Exp Syst Appl* 2015; 42: 5932–5946.
9. Yang S, Wang Z and Zhang H. Kinematic model based real-time path planning method with guide line for autonomous vehicle. In: *2017 36th Chinese control conference*, Dalian, China, 26–28 July 2017, pp.990–994. New York: IEEE.
10. Wang L, Zhao X, Su H, et al. Lane changing trajectory planning and tracking control for intelligent vehicle on curved road. *SpringerPlus* 2016; 5: 1150.
11. Cong Y, Sawodny O, Chen H, et al. Motion planning for an autonomous vehicle driving on motorways by using flatness properties. In: *Proceedings of the 2010 IEEE international conference on control applications*, Yokohama, Japan, 8–10 September 2010, pp.908–913. New York: IEEE.
12. Rasekhipour Y, Khajepour A, Chen S, et al. A potential field-based model predictive path-planning controller for autonomous road vehicles. *IEEE T Intell Transp Syst* 2017; 18: 1255–1267.
13. Suh J, Chae H and Yi K. Stochastic model predictive control for lane change decision of automated driving vehicles. *IEEE T Veh Technol* 2018; 67: 4771–4782
14. Li X, Sun Z, Zhu Q, et al. A unified approach to local trajectory planning and control for autonomous driving along a reference path. In: *Proceedings of the 2014 IEEE international conference on mechatronics and automation*, Tianjin, China, 3–6 August 2014, pp.1716–1721. New York: IEEE.
15. Nilsson J, Brannstrom M, Coelingh E, et al. Lane change maneuvers for automated vehicles. *IEEE T Intell Transp Syst* 2017; 18: 1087–1096.
16. Jeong hwan J, Cowlagi RV, Peters SC, et al. Optimal motion planning with the half-car dynamical model for autonomous high-speed driving. In: *2013 American control conference*, Washington, DC, 17–19 June 2013, pp.188–193. New York: IEEE.
17. Altché F, Polack P and deLa Fortelle A. A simple dynamic model for aggressive, near-limits trajectory planning. In: *2017 IEEE intelligent vehicles symposium (IV)*, Los Angeles, CA, 11–14 June 2017, pp.141–147. New York: IEEE.
18. Altché F, Polack P and de La Fortelle A. High-speed trajectory planning for autonomous vehicles using a simple dynamic model. In: *2017 IEEE 20th international conference on intelligent transportation systems (ITSC)*,

Yokohama, Japan, 16–19 October 2017, pp.1–7. New York: IEEE.
19. Delsart V, Fraichard T and Martinez L. Real-time trajectory generation for car-like vehicles navigating dynamic environments. In: *2009 IEEE international conference on robotics and automation*, Kobe, Japan, 12–17 May 2009, pp.3401–3406. New York: IEEE.
20. Dixit S, Fallah S, Montanaro U, et al. Trajectory planning and tracking for autonomous overtaking: state-of-the-art and future prospects. *Ann Rev Contr* 2018; 45: 76–86.
21. Kayacan E, Ramon H and Saeys W. Robust trajectory tracking error model-based predictive control for unmanned ground vehicles. *IEEE/ASME T Mech* 2016; 21: 806–814.
22. Petrov P and Nashashibi F. Modeling and nonlinear adaptive control for autonomous vehicle overtaking. *IEEE T Intell Transp* 2014; 15: 1643–1656.
23. Lei C, Chaofang H and Na W. Obstacle avoidance control of unmanned ground vehicle based on NMPC. In: *2017 Chinese automation congress (CAC)*, Jinan, China, 20–22 October 2017, pp.6402–6406. New York: IEEE.
24. Nehaoua L and Nouvelière L. Backstepping based approach for the combined longitudinal-lateral vehicle control. In: *2012 IEEE intelligent vehicles symposium*, Alcala de Henares, 3–7 June 2012, pp.395–400. New York: IEEE.
25. Xu T and Yuan H. Autonomous vehicle active safety system based on path planning and predictive control. In: *2016 35th Chinese control conference (CCC)*, Chengdu, China, 27–29 July 2016, pp.8889–8895. New York: IEEE.
26. Chebly A, Talj R and Charara A. Coupled longitudinal and lateral control for an autonomous vehicle dynamics modeled using a robotics formalism. *IFAC-PapersOnLine* 2017; 50: 12526–12532.
27. Zhou H, Güvenç L and Liu Z. Design and evaluation of path following controller based on MPC for autonomous vehicle. In: *2017 36th Chinese control conference (CCC)*, Dalian, China, 26–28 July 2017, pp.9934–9939. New York: IEEE.
28. Xu L, Wang Y, Sun H, et al. Design and implementation of driving control system for autonomous vehicle. In: *17th international IEEE conference on intelligent transportation systems (ITSC)*, Qingdao, China, 8–11 October 2014, pp.22–28. New York: IEEE.
29. Cai J, Jiang H, Chen L, et al. Implementation and development of a trajectory tracking control system for intelligent vehicle. *J Intell Robot Syst* 2019; 49: 251–264.
30. Norouzi A, Kazemi R and Azadi S. Vehicle lateral control in the presence of uncertainty for lane change maneuver using adaptive sliding mode control with fuzzy boundary layer. *Proc IMechE, Part I: J Systems and Control Engineering* 2017; 232: 12–28.
31. Guo J, Hu P and Wang R. Nonlinear coordinated steering and braking control of vision-based autonomous vehicles in emergency obstacle avoidance. *IEEE T Intell Transp Syst* 2016; 17: 3230–3240.
32. Choi J, Yi K, Suh J, et al. Coordinated control of motor-driven power steering torque overlay and differential braking for emergency driving support. *IEEE T Veh Technol* 2014; 63: 566–579.
33. Funke J, Brown M, Erlien SM, et al. Collision avoidance and stabilization for autonomous vehicles in emergency scenarios. *IEEE T Contr Syst Technol* 2017; 25: 1204–1216.
34. Attia R, Orjuela R and Basset M. Combined longitudinal and lateral control for automated vehicle guidance. *Vehicle Syst Dyn* 2014; 52: 261–279.
35. Liu J, Jayakumar P, Stein JL, et al. Combined speed and steering control in high-speed autonomous ground vehicles for obstacle avoidance using model predictive control. *IEEE T Veh Technol* 2017; 66: 8746–8763.
36. Bakker E, Nyborg L and Pacejka HB. Tyre modelling for use in vehicle dynamics studies. SAE technical paper 870421, 1987.
37. Rajamani R. *Vehicle dynamics and control*, 4th ed. New York: Springer, 2012.
38. Slotine J-JE. Sliding controller design for non-linear systems. *Int J Contr* 1984; 40: 421–434.

Appendix 1

Notation

$()_{f/r}$	front/rear axle
$()_{f/r,l/r}$	front/rear, left/right tyre
$()_{HV}$	host vehicle
$()_{R}$	reference value
$()_{TV}$	target vehicle
a	acceleration
A_F	frontal area of the vehicle
B, C, D	coefficient Pacejka's Magic formula
b_f, b_r	distance from CG to front/rear bumper
C_d	aerodynamic drag coefficient
CG	vehicle's centre of gravity
F_{aero}	aerodynamic drag force
f_r	rolling resistance coefficient
F_x, F_y	longitudinal/lateral tyre force
F_z	normal force on tyre
g	gravity acceleration
h	maximum lateral displacement of the HV
h_{aero}	height of the location at which the equivalent aerodynamic force acts
h_{CG}	height of CG
I_w	wheel's moment of inertia
I_z	vehicle yaw moment of inertia
k_b	braking gain
k_d	driveline gain (include final drive reduction)
k_{diff}	final gear reduction in the differential
$k_{x,b}, k_{x,t}, k_y$	uncertainty gain for braking, traction and lateral control, respectively
l	wheelbase
l_f, l_r	front/rear axle – CG distance
m	total mass of vehicle
P_b	brake master cylinder pressure
r_{eff}	effective radius of the tyres
s	total slip
$sat(.,.)$	saturation function
sd	lateral safe distance
s_x, s_y	longitudinal/lateral slip
ss_x, ss_y	longitudinal/lateral sliding surface

s_0	initial inter-vehicle distance	$\dot{\omega}$	wheel angular speed
T_b	total wheel braking torque	ρ	mass density of air
t_c	moment that the HV reaches to the TV	β	vehicle slip angle
T_d	total wheel driving torque	δ	front-wheel steering angle
T_e	net engine torque	α	tyre slip angle
t_f	lane change duration	ψ	vehicle yaw angle
T_r	rolling resistance torque	$\dot{\psi}$	vehicle yaw rate
t_w	track width	$\ddot{\psi}$	yaw angular acceleration
v	total velocity at CG	μ	friction coefficient
v_{cw}	wheel ground contact point velocity	ω_e	rotational engine speed
v_{rw}	rotational equivalent wheel velocity	η_d	driveline efficiency
v_{wind}	wind speed	η_g	transmission gear ratio
v_x, v_y	longitudinal/lateral velocity at CG	α_{th}	throttle opening
v_0	initial speed of host/TV	τ_b	time constant of the brake actuator
w	vehicle width	ϕ_x, ϕ_y	boundary layer thickness for longitudinal/lateral control
(X, Y)	CG's position in inertial coordinates		
(x, y)	body-fixed coordinates	$\eta_x, \eta_y, \lambda_x, \lambda_y$	strictly positive constants
ω	wheel angular speed		